# Efficient and accurate assessment of window view distance using City Information Models and 3D Computer Vision

Maosu Li[1], Fan Xue[2], and Anthony G. O. Yeh[3*]

## Abstract

A distant view through a window is preferred by urban dwellers due to its benefits to human health and well-being. A high window view distance is also valued in real estate markets, especially in high-rise, high-density urban areas. Thus, an urban-scale assessment of window view distance is significant in examining the disparity of sharing of view openness for applications and analytics in urban health, planning and design, and housing. However, current limited assessment methods are neither accurate nor efficient. The evolving photorealistic City Information Models (CIMs) and 3D Computer Vision (CV) enable a new solution due to the high-resolution and efficient semantic representation of urban landscapes. This study aims to present a window view distance index (WVDI) together with an accurate and efficient assessment method using up-to-date 3D CIMs and CV. First, we define the WVDI on a CIM-generated window view image considering the visual permeability of greenery. Then, an automatic assessment of WVDIs is designed on a type-depth window view using 3D semantic segmentation and OpenGL rendering. Experimental tests in Hong Kong Island and Kowloon Peninsula of Hong Kong confirmed that our method was i) accurate for both non-greenery views (RMSD ≤ 0.0002) and greenery views (RMSD ≤ 0.1781) and ii) improved the efficiency of the traditional visibility analysis-based method by 99.96%. The proposed approach can support multiple urban applications, e.g., prioritized improvement of visual urban density, overall optimization of

---

[1] Maosu LI, Post-doctoral Fellow.
Department of Urban Planning and Design, The University of Hong Kong, Pokfulam, Hong Kong, China;
Email: maosuli@hku.hk, : https://orcid.org/0000-0002-9970-4053

[2] Fan XUE, Associate Professor.
Department of Real Estate and Construction, The University of Hong Kong, Pokfulam, Hong Kong, China;
National Center of Technology Innovation for Digital Construction Hong Kong Branch, The University of Hong Kong, Pokfulam, Hong Kong, China;
Email: xuef@hku.hk, : http://orcid.org/0000-0003-2217-3693

[3] Anthony G. O. YEH, Chair Professor.
Department of Urban Planning and Design, The University of Hong Kong, Pokfulam, Hong Kong, China;
Email: hdxugoy@hku.hk, : http://orcid.org/0000-0002-0587-0588
*: Corresponding author, Tel: +852 3917 2721 Email: hdxugoy@hku.hk

window view distance for architectural and urban design, and precise housing valuation and transaction.

## Keywords

Window view; View distance; View openness; Visual permeability; City information model; Computer vision

## 1 Introduction

A distant view through a window is preferred by urban dwellers (Kent & Schiavon 2020; Lin et al. 2022), especially in high-rise, high-density cities, e.g., Hong Kong (Fisher-Gewirtzman 2018; Wang & Munakata 2024). The high window view distance and openness benefit urban dwellers' health and
30　well-being through stress relief, living satisfaction, and productivity improvement (Chung et al. 2019; van Esch et al. 2019; Luo & Jiang 2022). Another benefit is providing urban dwellers with an increased sense of privacy in the crowded urban environment (Fisher-Gewirtzman 2018; Ko et al. 2022). In this study, "window view distance" refers to the average distance between the window center and all the visible landscape objects outside (see Figure 1e). In the post-Covid-19 era, the benefits of distant views through windows become prominent due to long-term staying at home and workplaces (McPhail et al. 2024). By contrast, narrow rooms without windows or with close-range views of building facades can lead to the occupants' mental disorders, stress, and depression (Ulrich 1984; Chung et al. 2019). Thus, an urban-scale assessment of window view distance is significant in examining the disparity of sharing of view openness, particularly for healthy high-rise, high-density
40　urban development.

Urban-scale assessment of window view distance enables multiple urban applications and analytics. First, window view distances represent visual urban density that urban dwellers experience long-term from their residences and offices (Fisher-Gewirtzman 2018; Li et al. 2024). The disparity of assessed window view distances can help urban planners identify the buildings and blocks with high local urban density for prioritized improvement (Masoudinejad & Hartig 2020). The assessed window view distance can support generative architectural and urban design to achieve maximized sharing of window view openness (Laovisutthichai et al. 2021; Kim et al. 2022; Wang et al. 2024; 2025). Additionally, the quantified window view distance can support both property agents' precise housing valuation and the purchasers' and renters' housing selection. Last, the assessed window view distance
50　can be correlated with urban mental health issues, e.g., stress and depression (van Esch et al. 2019; Masoudinejad & Hartig 2020) for advancing environmental justice and urban sustainability.

Researchers have assessed urban view distance through visibility analysis. For instance, the openness of natural and urban open spaces was examined for urban management (Tong et al. 2020; Zhu et al. 2024), while the distances between window sites and visible landscape outside were assessed for

urban and architectural design (Fisher-Gewirtzman 2018; Kim et al. 2022). However, current limited assessments of window view distance are neither accurate nor efficient. First, high-resolution 3D CIMs, e.g., photorealistic CIMs and point clouds, are scarcely utilized for an accurate assessment due to high time-cost processing (Inglis et al. 2022; Li et al. 2024). Thereafter, landscape elements are all modeled as solid surfaces, although certain elements, e.g., greenery, are porous and visually permeable in nature (Bartie et al. 2011; Ruzickova et al. 2021). The inaccuracies and inefficiencies of current methods are magnified, especially in densely developed urban areas due to the complex 3D landscapes. Thus, the research question of the study is:

> "*Regarding the visual permeability of landscape elements, how to efficiently and accurately assess window view distance using up-to-date photorealistic CIMs for urban applications?*"

This study introduces a window view distance index (WVDI) together with an accurate and efficient assessment method using photorealistic CIMs and 3D computer vision. A 3D visualization of WVDI based on Building Information Models (BIMs) is presented for applications in urban planning and design and real estate marketing.

The main contribution of this study is twofold.

i. Theoretically, a novel WVDI is defined on a photorealistic CIM-generated window view image regarding the visual permeability modeling of greenery. The defined WVDI challenges and extends the traditional assessment results of window view distances on both oversimplified and solid surface models.

ii. The proposed method conducted on the 3D CIM-generated type-depth window views is automatic and efficient in assessing window view distances at the urban scale. The assessment results are accurate for planners, designers, and government policymakers in urban planning and design, as well as housing purchasers, renters, and property agencies in the real estate market.

We present the remainder of this study as follows. The literature is reviewed in Section 2. Section 3 presents the definition of WVDI, the automatic assessment of WVDI, and a 3D BIM-based visualization of WVDI. Experimental tests were conducted in Section 4. Sections 5 and 6 present the discussion and conclusion, respectively.

## 2 Literature review

### 2.1 Roles of distant views' benefits and impacts for automatic assessment

Researchers in psychology, built environment, and urban studies have examined the benefits of distant views on human health and well-being. Compared to close-range views, distant views through windows provide urban dwellers with high-level openness and spaciousness (Stamps III 2011; Yao et al. 2024). Recognized benefits of distant views include visual fatigue relief and post-surgical recovery

for physical health (Ulrich 1984; Kent & Schiavon 2020; Lin et al. 2022) as well as stress and

90 depression relief for mental health (Masoudinejad & Hartig 2020; Luo & Jiang 2022). The benefits of distant window views for human health and well-being underscore the value of quantification of window view distance.

The impacts of distant views through windows are found in real estate marketing and urban planning and design. For instance, by comparing flats online or in-person, housing purchasers and renters are willing to pay a premium for openness provided by sky and sea views (Huang 2019; Masoudinejad & Hartig 2020; Ling 2022). As a result, property agents often manually identify flats with high window view openness in the property market for extra profits (Yamagata et al. 2016). Additionally, a satisfactory window view distance has been recommended for architectural design in Europe (CEN 2018) and the US (IWBI 2020). Window view openness is optimized by architects via improving the

100 building envelope and room layouts (Kim et al. 2022; Ko et al. 2022). Visual densities in city blocks regarding window view distances have been tried to be improved by urban planners and designers (Fisher-Gewirtzman 2018). The impacts of window view distances in housing, urban planning, and design practices enhance the need for automatic assessment.

## 2.2 Current assessment of window view distance

Current assessment of window view distance is limited, inaccurate, and inefficient. Researchers in psychology, built environment, and architectural design manually measured window view distances through onsite experiments or 2D maps (Stamps III 2011; Kent & Schiavon 2020). The high labor cost is unscalable to the urban scale. Additionally, the amount of sky view seen from the window is considered a proxy for view openness (Masoudinejad & Hartig 2020; Li et al. 2022). However, only

110 the composition of view types cannot identify the slight difference in view distance. Examples are window views with the same proportion of sky but varied landscape distances.

In the fields of Geographic Information Science (GIS) and urban planning, traditional visibility analysis such as viewshed and *isovist* enabled the measurement of window view distance at the urban scale (Fisher-Gewirtzman 2018). However, the large-scale assessment methods for window view distances are limited and prone to errors regardless of the efficiency. First, current assessments often fail to represent the real urban landscape using oversimplified 2.5/3D models (Mistick et al. 2023; Li et al. 2023b). For instance, blended objects, e.g., constructions and greenery in the real urban landscape, are often modeled by discrete cubic buildings, identical fake trees, and 2.5D Digital Terrain Models (DTMs) (Inglis et al. 2022; Qi et al. 2022). On the contrary, high-resolution 3D CIMs

120 are less utilized due to high time-cost processing (Inglis et al. 2022; Li et al. 2024). Thereafter, all landscape elements are consistently modeled using solid surfaces, overlooking the visual permeability of certain landscape elements, e.g., porous foliage of greenery (Bartie et al. 2011; Ruzickova et al. 2021). For instance, porous tree foliage, when modeled as a solid green wall, can completely obstruct

the sightlines from nearby windows, resulting in negligible errors in view distance (Fisher-Gewirtzman 2018).

## 2.3 Visual permeability modeling of greenery and semantic representation of CIMs

Visual permeability modeling of greenery has been developed for visibility analysis in GIS and landscape management. Researchers argue greenery modeled as solid 2.5D triangle meshes or 3D convex hulls is unrealistic and prone to errors (Llobera 2007; Zong et al. 2021; Mistick et al. 2023).

130 To estimate the visual permeability of greenery, the classic Beer-Lambert's Attenuation Law (Swinehart 1962) in physics was introduced by Llobera (2007). Greenery, e.g., trees, was structured as a set of thin and porous slices. The potential extra view distance depends on the thickness and porosity of the slices. Llobera's (2007) formula based on Beer-Lambert's Attenuation Law (Swinehart 1962) has been used in the permeability modeling in landscape management and ecological research (Bartie et al. 2011; Murgoitio et al. 2013; Ruzickova et al. 2021)

Evolving 3D urban visual intelligence (Zhang et al. 2024), e.g., semantic representation techniques, enable accurate and efficient assessment of window view distance. First, 3D photorealistic CIMs can generate high-resolution window views similar to those captured in the real world (Li et al. 2021; 2022). 3D semantic segmentation of photorealistic CIMs can automatically identify city objects, e.g.,

140 ground, building, and greenery (Li et al. 2023a), for urban studies, e.g., landscape view assessment (Qi et al. 2022; Li et al. 2023b), urban infrastructure digitalization (Meng et al. 2025), and construction safety (Liang et al. 2024). Last, OpenGL rendering in 3D computer graphics enables both efficient and semantic-enriched visualization of 3D photorealistic CIMs (Li et al. 2023b).

In summary, an accurate and efficient assessment of window view distance is significant for urban applications, yet it is lacking in current studies. Two observed issues are the high processing cost of high-resolution 3D CIMs and consistent solid landscape surface modeling regardless of the visual permeability of greenery. Meanwhile, the up-to-date photorealistic CIMs, 3D semantic segmentation, and OpenGL rendering open up new opportunities for an automatic, accurate, and efficient assessment of window view distance.

150 This study aims to present a window view distance index (WVDI) together with an accurate and efficient assessment method. We model the visual permeability of greenery on a photorealistic CIM in defined WVDI. Leveraging 3D semantic segmentation and OpenGL rendering of CIM, the accuracy and efficiency of the automatic assessment are improved through a type-depth window view integration.

## 3 Research methods

Figure 1 shows the research framework of the proposed WVDI together with the automatic assessment method. The inputs comprise 3D photorealistic CIMs, BIMs, DTM, and density

parameters of greenery (see Figure 1a). The proposed assessment method comprises two parts: i)

definition of WVDI on a photorealistic CIM-generated window view image regarding visual

160    permeability of greenery (see Figure 1b), and ii) automatic computation of WVDI using 3D semantic

segmentation and OpenGL rendering. Specifically, the automatic computation method comprises

three steps: i) landscape type estimation of photorealistic CIMs using 3D semantic segmentation (see

Figure 1c), ii) type-depth landscape scene rendering through OpenGL shading (see Figure 1d), and iii)

batch generation and quantification of window views for WVDIs (see Figure 1e). Last, BIM-based

visualization of WVDIs (see Figure 1f) is presented for urban applications such as local urban density

improvement and informed housing valuation and transaction. The final output is a set of visualized

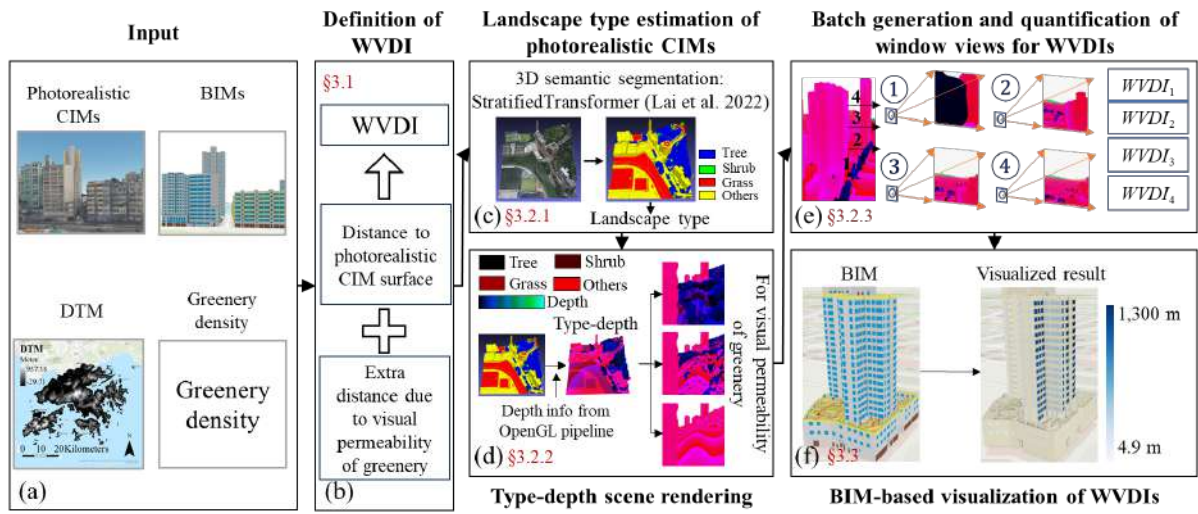WVDIs coded with geolocations of window sites.



**Figure 1.** Research framework. (a) Input, (b) definition of WVDI, (c)-(e) a three-step automatic

170    assessment method, and (f) visualized WVDIs on BIMs.

## 3.1 Definition of window view distance index (WVDI)

WVDI in this study is defined on a simulated window view image generated on the photorealistic

CIMs. The example window view image (see Figure 2a), generated from the window center, presents

the landscape scene that a normal adult mainly sees when looking out horizontally. Regarding the

visual permeability of greenery (see Figure 2b), WVDI is the average pixel-level depth of the CIM-

generated window view image using Equation (Eq.) 1.

$$WVDI = \Sigma_{i = 1, 2, \ldots n} D_i / n, \tag{1}$$

$$D_i = \begin{cases} d_i^s + w_i(d_i^m) \times d_i^p + (1-w_i(d_i^m)) \times \int_0^{d_i^m} x \times w_i(x)\, dx, & \text{if } c(i) = \text{greenery, e.g., tree, shrub, grass,} \\ d_i^s, & \text{if } c(i) = \text{other landscape elements and sky,} \end{cases} \tag{2}$$

where $D_i$ is the depth of the view elements on pixel $i$ of the window view image. $n$ is the total number

of image pixels. $c$ is the class of the window view elements, e.g., the tree, shrub, grass, other

landscape elements, and sky. $d_i^s$ and $d_i^p$ are view depths corresponding to surface and penetration, respectively, as shown in Figure 2c, whereas $d_i^m$ is the depth of the greenery alongside the sightline. $w_i(d_i^m)$ and $1 - w_i(d_i^m)$ represent the probabilities of the sightline penetrating or being absorbed within the greenery, respectively. Since sightline may stop within greenery at a random value of transmission length $x$ $(0 \leq x \leq d_i^m)$, we apply the integral function, $\int_0^{d_i^m} x \times w_i(x) \mathrm{d}x$, to calculate the expectation value of view depth for the absorption. Note that the usage of penetration and absorption in Eq. 2 depends on the percentage of greenery window views in the assessment area. For example, there existed accuracy improved for assessing greenery window views (83.57%) and particularly close-range ($\leq 30$ m) greenery views (18.27%) in the study area (see Section 4). For other landscape elements and sky, only $d_i^s$ is calculated. Particularly, $d_i^s$ for the sky can be a fixed depth parameter, i.e., $\alpha$, set by researchers and practitioners.
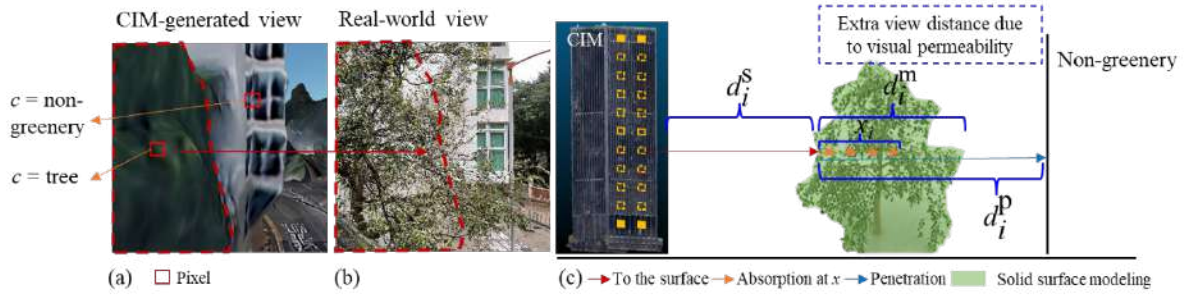


**Figure** 2. Comparison of (a) CIM-generated and (b) real-world window views, and (c) three typical sightlines from the window to the greenery.

According to the literature review in Section 2.3, Llobera's (2007) formula based on Beer-Lambert's Attenuation Law (Swinehart 1962) is applied in Eq. 3 to estimate the sightline's penetration probability $w(d^m)$,

$$w_i(x) = \begin{cases} (1 - f_{c(i)})^x, & c(i) = \text{greenery, e.g., tree, shrub, grass, } 0 \leq f_{c(i)} \leq 1, \\ 0, & c(i) = \text{non-greenery, e.g., other landscape elements and sky,} \end{cases} \tag{3}$$

where $f_c$ is the average density of a certain type of greenery as one of the four inputs (see Figure 1).

### 3.2 Automatic computation of WVDI using 3D colored City Information Models

#### 3.2.1 Landscape type estimation of photorealistic CIMs using 3D semantic segmentation

Computation of WVDI requires both the type $c$ and depth $d$ of each pixel of the CIM-generated window view image according to Eq. 1 to 3. Thus, we estimate the landscape type $c$ of photorealistic CIMs through a three-step workflow. First, landscape type $c$ of photorealistic CIMs was estimated from the sampled point clouds. Making full use of publicly available deep learning methods and training datasets of point clouds, we segment the sampled point clouds (see Figure 3a) into two categories: greenery and non-greenery (see Figure 3b). The most high-performance 3D semantic segmentation method validated in Section 4.3.1, namely, StratifiedTransformer (Lai et al. 2022) is

applied for greenery detection. Example subtypes of greenery, i.e., grass, shrubs, and trees are then differentiated by their heights. The greenery height $h$ is represented as the elevation difference between the greenery surface and the terrain or building roof where it is located. Eq. 4 shows the A-priori rules, where the thresholds $\beta$ and $\gamma$ are set as 0.9 m and 4 m according to the sensitivity analytical result in Section 4.3.2. Example segmented point clouds are shown in Figure 3c.

$$c = \begin{cases} \text{tree,} & \gamma \leq h \\ \text{shrub,} & \beta \leq h < \gamma \\ \text{grass,} & 0 \leq h < \beta. \end{cases} \tag{4}$$

Secondly, we remove the textures of the photorealistic CIM (see Figures 3d and e). The textureless CIM is for both segmentation result loading and the landscape scene rendering in Section 3.2.2. Last, the segmented point clouds are registered to the textureless CIM to estimate the landscape type of each triangular face. The output is CIM colored by estimated landscape types (see Figure 3f).
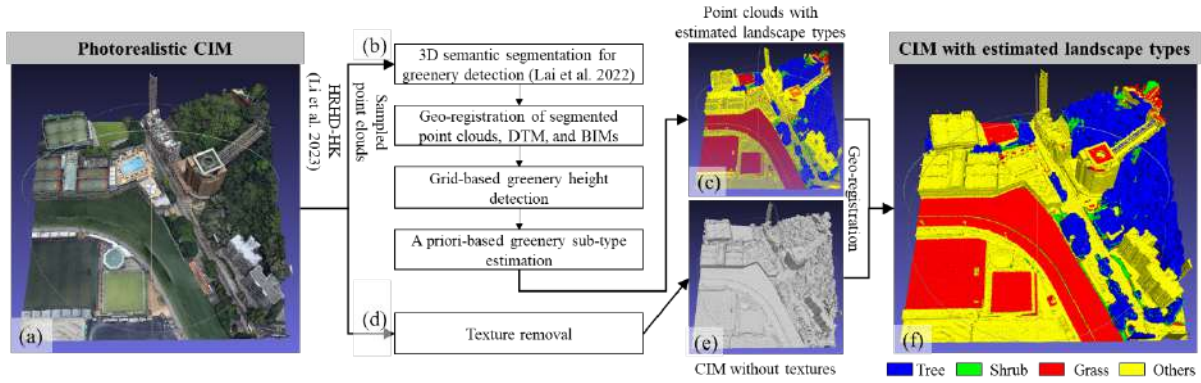


**Figure** 3. Workflow of landscape type estimation. (a) Photorealistic CIM as input, (b) greenery detection of (c) sampled point clouds using 3D semantic segmentation, (d)-(e) texture removal of photorealistic CIMs, and (f) CIM geo-registered with estimated landscape types.

*3.2.2 Type-depth scene rendering through OpenGL shading*

By collecting depth $d$, we integrate the estimated landscape type $c$ and view depth $d$ on a 3D scene using OpenGL shading. First, the 3D textureless CIMs (see Figure 4a) are loaded on the digital terrain of a 3D geo-visualization platform, e.g., Cesium. Figure 4b shows the estimated landscape type $c$ of the CIM from Section 3.2.1 and the pixel-level depth $d$ collected from the depth buffer test of the OpenGL rendering pipeline. Then, the OpenGL fragment shader is set for a colored scene that depicts landscape type $c$ and view depth $d$ simultaneously. Specifically, the R value of the scene represents estimated landscape type $c$ (see Figure 4b). The R value ranges between 0 and 255, representing at most 256 types of landscape elements. To explicitly visualize the different types of landscape, we set R values to 0, 80, 160, 240, and 255 to represent trees, shrubs, grass, other landscapes, and sky, respectively, as shown in Figure 4c. Meanwhile, we regard the G and B values of the scene as tens

and ones place of the 256-base number to represent the view depth $d$. The 256-base number ranges between 0 and 65,535, which can represent varied view depth ranges with different accuracy. For example, setting the maximum view depth at 65,535 m corresponds to 1-m accuracy, whereas setting the maximum view depth at 6,554 m corresponds to an accuracy of 0.1 m. At the accuracy of 0.1 m, Figure 4c shows a type-depth scene by dynamically rendering values of R, G, and B for each pixel. Particularly, we represent $d^s$ on the 3D scene without extra settings (see Figure 4d), and represent $d^s + d^m$ and $d^s + d^p$ on the 3D scene by inversing the normal of triangular faces of greenery and setting their visibility off, respectively (see Figures 4e and f).
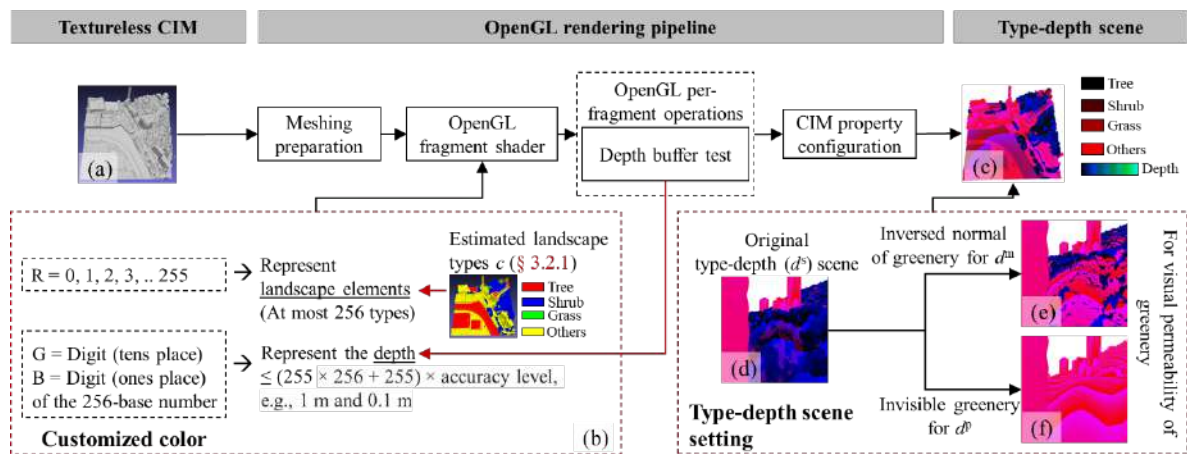


**Figure** 4. Pipeline of type-depth scene rendering through OpenGL shading. (a) Textureless CIM, (b) customized shading of CIM, and (c)-(f) rendered type-depth scenes representing depths $d^s$, $d^m$, and $d^p$.

### *3.2.3 Batch generation and quantification of window views for WVDIs*

Last, the type-depth window views are generated from the rendered type-depth scene for computing WVDIs. Specifically, we set the parameters of the virtual camera function of a 3D geo-visualization platform, e.g., Cesium, to capture the window view (see Figure 5b). The 3D coordinates, e.g., *lon*, *lat*, and *elevation*, of the window center from BIMs (see Figure 5a) are used to place the virtual camera, while rotation parameters, i.e., *heading*, *pitch*, and *roll*, of the virtual camera are adjusted to align with the window orientation. The field of view, e.g., 60 degrees, and the image aspect ratio of the virtual camera, e.g., 1:1, are set to capture the landscape elements that a normal adult mainly sees from the window center. Note that researchers and practitioners can adjust the virtual camera's parameters, e.g., 3D coordinates, rotation, field of view, and image aspect ratio, which change WVDI values, to capture their desired views of windows with varying sizes and height-width ratios. By repetitively placing the virtual camera at each window center in the rendered type-depth scene (see Figure 5d), type-depth window views are automatically generated (see Figure 5e). Last, landscape type $c$ and view depth $d$ are decoded from the R, G, and B values of the window view image to compute WVDI (see Figure 5f) using Eq. 5, 6, and 1.

$$c(i) = \begin{cases} \text{tree,} & \text{if } R_i = 0, \\ \text{shrub,} & \text{if } R_i = 80, \\ \text{grass,} & \text{if } R_i = 160, \\ \text{others,} & \text{if } R_i = 240, \\ \text{sky,} & \text{if } R_i = 255, \end{cases} \tag{5}$$

$$d_i = (G_i \times 256 + B_i) / 10 \text{ if } c(i) \in \{\text{tree, shrub, grass, other landscape elements}\} \text{ else } \alpha, \tag{6}$$

where $\alpha$ is the depth parameter of the sky set by researchers and practitioners for computing WVDIs.
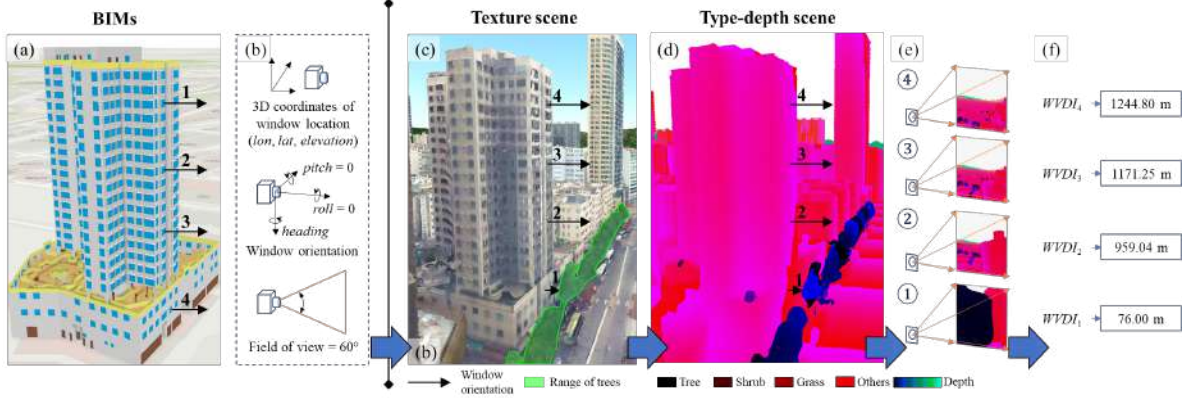


**Figure** 5. Batch generation of type-depth window views for WVDIs. (a) BIMs as input, (b) parameter setting of the virtual camera function, (c)-(d) texture and type-depth scenes, and (e)-(f) generated type-depth views and WVDIs.

### 3.3 BIM-based 3D visualization of WVDI

We visualize WVDIs on geo-registered BIMs (see Figure 6a) for urban applications, e.g., local urban density improvement and housing valuation and transaction. First, windows and other components of BIMs are separated (see Figures 6b and d). Then, we color the vertexes of window polygons using WVDIs (see Figure 6c). We use the maximum and minimum WVDIs of the buildings in the study area to determine the range of the color bar. By contrast, the color of other components is unified to serve as the background (see Figure 6e). Last, we re-integrate colored windows and other background components to construct a 3D map of WVDIs (see Figure 6f). The dark blue indicates a high WVDI, whereas the light blue represents a low view distance of the window.
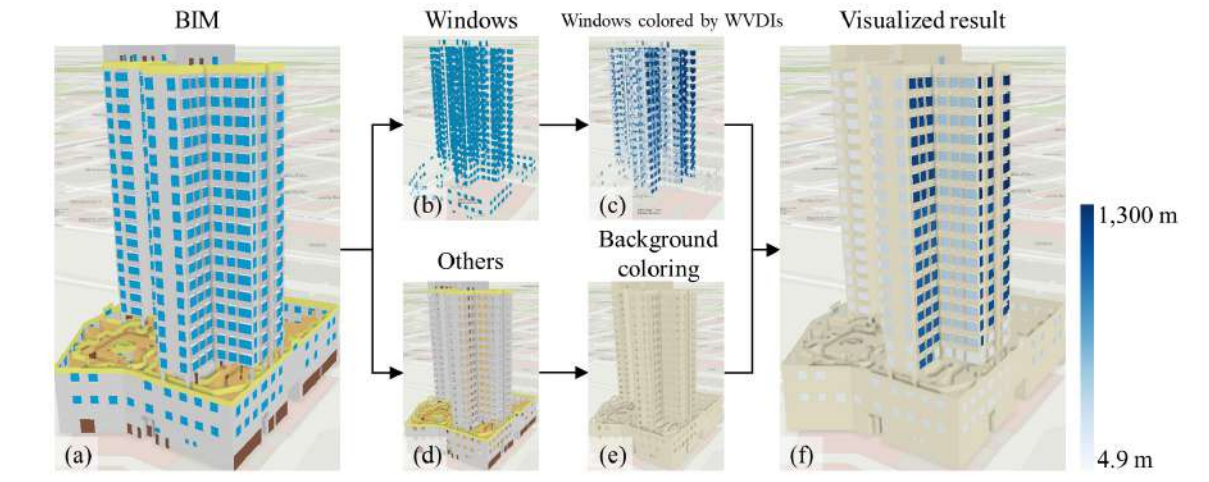
**Figure** 6. Visualization of WVDIs based on BIMs. (a) BIMs as input, (b)-(c) extracted windows colored by WVDIs, (d)-(e) other components colored as background, and (f) visualized result.

## 4 Experimental tests

### 4.1 Experimental area and settings

We chose high-rise, high-density urban areas in Hong Kong Island and Kowloon Peninsula of Hong Kong, as the study area (see Figure 7a). The average building height reaches 23.92 m, whereas the site coverage of the study area is 0.8 (HKPlanD 2018). With the compact urban settings, the greenery blends with high-rise buildings and other landscapes. View distances of windows vary by their floor height and orientations. Figure 7c shows the photorealistic CIMs collected from the Hong Kong Planning Department (2019). Window locations were sampled from the building datasets shared by the Hong Kong Lands Department (2023) and the Urban Renewal Authority (2022). Annotated point clouds, the HRHD-HK (Li et al. 2023a) in Hong Kong were applied to train the StatifiedTransformer for landscape type estimation in Section 3.2.1. A 0.5-m DTM (HKLandsD 2020) represented the terrain in Sections 3.2.1 and 3.2.2. The average densities for trees, shrubs, and grass collected from the field test were finetuned to 0.7, 0.8, and 0.9 for a high assessment accuracy, according to the sensitivity analytical result in Section 4.3.3.
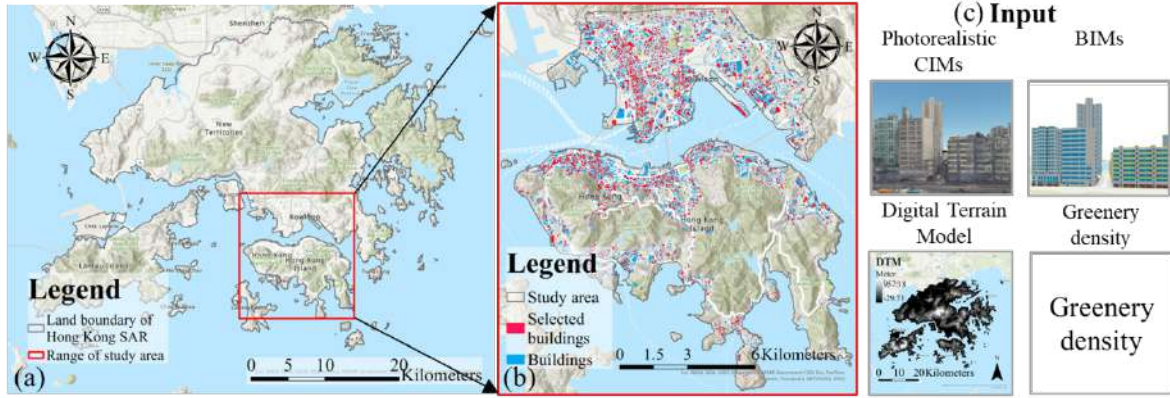
**Figure** 7. (a) Study area, (b) 4,805 randomly sampled buildings, and (c) four inputs of the proposed method.

We sampled 73,512 window view images from 4,805 buildings (see Figure 7b) in the study area to assess the proportion of close-range greenery window views. Window view images were first classified by landscape view distance and the presence of greenery into $7 \times 2$ categories. Considering the impact of the visual permeability of greenery, especially for close-range window views, we classified view distances in meters into seven categories, i.e., (0, 5], (5, 10], (10, 15], (15, 20], (20, 25], (25, 30], (30, 2,279). We used 5 m as an interval to classify close-range ($\leqslant$ 30 m) window views, regarding the high-rise, high-density context of the study area. The dummy variables for the presence of greenery were set to 0 and 1. Figure 8b showed around 3% of the total number of samples existed at every 5-m interval for greenery window views. Then, we extended the dummy variables into five categories, i.e., [0, 0.2), [0.2, 0.4), [0.4, 0.6), [0.6, 0.8), and [0.8, 1], to examine our method's efficiency and accuracy. With one window view image randomly collected from each category, we computed WVDIs of 35 window view images using both our method and the typical 3D visibility analytical tool, Line of Sight (LoS) of ArcGIS Pro (ver. 2.9.0), for comparison. Specifically, we generated each window view in a RGB image with $900 \times 900$ pixels. The field of view was 60 degrees to represent what urban dwellers mainly see from the center of the window. Meanwhile, an in-house LoS program using ArcPy (ver. 2.9.0) was developed to assess the distance between the window center and the landscape within a 60-degree viewing frustum, using $900 \times 900$ samples. To preliminarily test the feasibility of the proposed method, we set the distance to sky $\alpha$ as 2,000 m (Qi et al. 2022) for computing WVDIs. The maximum view depth for G and B channels is 6,336 m to retain the accuracy at the 10th percentile.

The experiments were implemented in the workstation with a 16-core Intel i9-11900K CPU, a 24G Nvidia GeForce RTX 3090 graphic card, 64GB memory, and a Windows 10 system (64-bit). We implemented the 3D semantic segmentation in a docker container with Pytorch (ver. 1.10.0), making full use of the CPU and GPU resources of the workstation. Editing of CIM, e.g., normal setting of

triangular faces of greenery, was implemented using the PyMeshLab (ver. 1.0.2). The type-depth scene of the textureless CIMs was rendered on a 3D geo-visualization platform, Cesium (ver. 1.99). Last, the WVDIs were computed through a Python (ver. 3.7.11) program and visualized on BIMs loaded in ArcGIS Pro (ver. 2.9.0).

## 4.2 Results

320    Figure 8 shows the distribution of the window views according to the greenery view proportion and average landscape view distance. Figure 8a shows most sampled window views contained greenery, while varied proportions of greenery existed in close-range ($\leq$ 30 m) window views. Statistically, the greenery window views accounted for 83.57% of the whole samples (see Figure 8b), whereas the close-range ($\leq$ 30 m) greenery window views took up 18.27%. The presence of greenery window views as a majority and the substantial existence of close-range greenery window views both reflected the significance of our method.
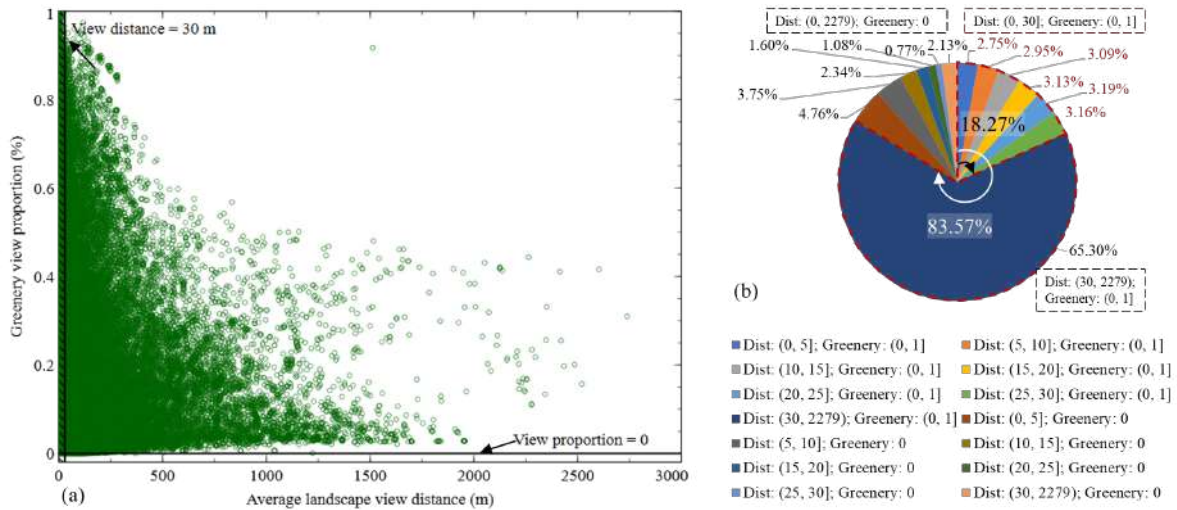


**Figure** 8. Distribution of sampled window views by average landscape view distance and greenery view proportion.

330    Table 1 compares the efficiency of the LoS analysis-based window view assessment and the proposed method. The LoS analysis consumed 10,350 seconds to measure the distance between the window center and 810,000 samples of the landscape scene through sequential ray tracing. By contrast, our method's rendering of the full type-depth landscape scene at one time consumed 0.5 seconds, which improved the efficiency of the LoS analysis by 99.99%. Furthermore, the LoS analysis failed to measure the depths of probabilistic penetration and absorption without the visual permeability modeling of the greenery (see Table 1). On the contrary, our method consumed 0.56 seconds and 2.68 seconds for probabilistic penetration and absorption within greenery, respectively. Overall, our method consumed 3.76 seconds for the WVDI of each window view image, improving the efficiency of the LoS analysis by 99.96%.

**Table 1.** Comparison of computational time ($t$) of the LoS analysis and the proposed method (The average for 35 selected window view images)

| No. | Depth type | $d$ in WVDI (Eq. 1&2) | LoS | $t$ (s) | Proposed method | $t$ (s) | Improvement |
|---|---|---|---|---|---|---|---|
| 1 | Surface | $d^s$ | Sequential ray tracing | 10,350 | OpenGL rendering | 0.50# | 99.99% |
| | | | | | Image array computing | 0.02 | |
| 2 | Probabilistic penetration | $w(d^m) \times d^p$ | / | / | OpenGL rendering | 0.50# | / |
| | | | | | Image array computing | 0.06 | |
| 3 | Probabilistic absorption | $(1 - w(d^m))$ $\times \int_0^{d^m} x \times w(x)\mathrm{d}x$ | / | / | OpenGL rendering | 0.50# | / |
| | | | | | Image array computing | 2.18 | |
| | | | Total | 10,350 | Total | 3.76 | 99.96% |

\# The average time depends on the setting of the time interval for the sequential generation of window view images.

Figure 9 shows our method's improvement in distance assessment because of the visual permeability modeling of greenery. For window views without greenery, the WVDI computed by our method was consistently close to the measured WVDI from the LoS analysis, as shown in the orange rectangle of Figure 9a. The absolute deviation (Dev.) and the Root Mean Squared Deviation (RMSD) were less than 0.01 m and 0.0002, respectively. The possible reason for the deviation was the retainment of the

accuracy to the 10th percentile of the rendered type-depth scene set in Section 4.1. For greenery window views, substantial positive deviations (Dev. $\geq 0.2893$) existed between the results of the LoS and our method. Particularly, the deviations for 71.43% of greenery window views exceeded 1.03 m, as shown in the red rectangle of Figure 9a. There existed a small improvement in the assessed view distance for the last eight greenery window views. With similar proportions of greenery views, possible reasons are i) low visual permeability rate $w(d^m)$ (denoted as $w$ in the following parts) and the $d^p$ or ii) mismatching of high values of $w$ and $d^p$ at the pixel level. For example, compared to other window views with greenery proportions ranging from 0.2 to 0.4, the improvement for window view #1 at 0.29 was the smallest due to both low $w$ and $d^p$. With similar values of $w$ and $d^p$, the improvement for window view #2 was 2.21% of that of window view #3 due to the mismatching of

high values of $w$ and $d^p$ at the pixel level.

Figure 9b shows the defined WVDI matters, especially for greenery window views with low $d^s$ and high visual permeability rate $w$ and $d^p$. With low $d^s$, Figure 9b shows the assessed distances of eight close-range greenery window views, indicated by red arrows, improved by more than 12.43%. The assessed WVDIs effectively represented the extra window view distance due to the visual permeability of the greenery, e.g., sparse tree foliage in front of the windows. Additionally, with relatively high $d^s$, three window views, indicated by black arrows, also owned high adjustment ratios above 9.58% due to high visual permeability rate $w$ and $d^p$. The high adjustment ratios further reflected that the modeling of visual permeability isr significant in accurately assessing window view distances, even for distant window views.
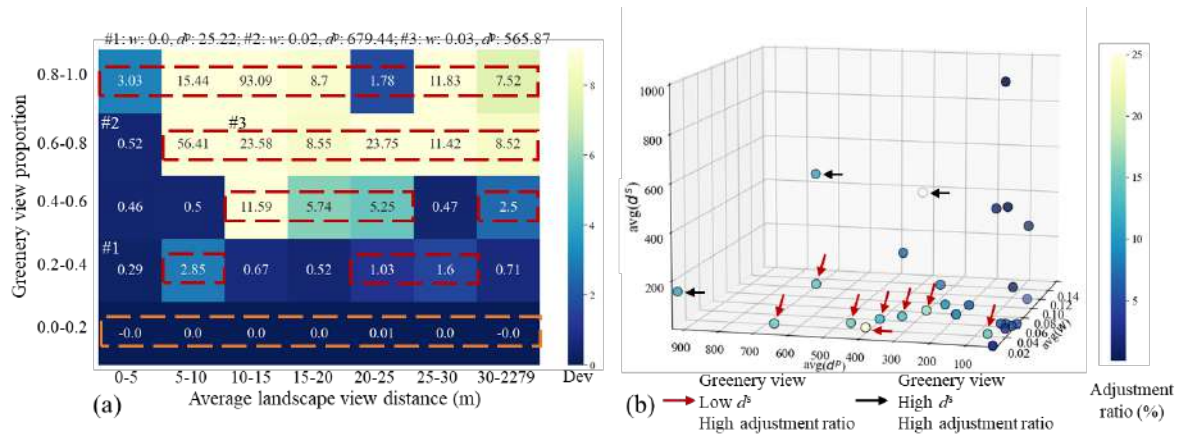
370



**Figure** 9. (a) Assessment accuracy of the proposed method compared to the ArcGIS Pro LoS analysis and (b) comparison of adjustment ratios for greenery window views.

Figure 10 illustrates ten example window views with different WVDIs, categorized into non-greenery (proportion = 0) and greenery (proportion > 0). The WVDI computed by $d^s$ for non-greenery views effectively represented the view distances. Window views #3, #4, and #5 with the sky elements were more distant than the window views #1 and #2. The view distances for windows #1 and #2 against pure building walls were differentiated, with the gap at 18.59 m. By contrast, the WVDIs for greenery views were larger than $d^s$ regarding the visual permeability of greenery. The differences were less than 1.78 m for window views #6, #7, and #9 due to the close-range building or terrains behind the greenery. On the contrary, there existed a high adjustment ratio ($\geq$ 10.00%) of assessed view distances for window views #8 and #10 due to potentially large amounts of the sky behind the greenery.



**Figure** 10. Typical (a) non-greenery and (b) greenery window views with WVDIs.

Figure 11 shows the visualized WVDIs on BIMs of 207 example buildings in To Kwa Wan, Kowloon City District. The visualized WVDIs can support multiple applications in urban planning and design

and real estate marketing. For instance, aging buildings #1 with consistently low WVDIs can be first considered by urban planners and designers for redevelopment. For building #2, slight differences in WVDIs between floors #1, #2, #3, #4, and #5 can support precise housing valuation by property agents, whereas tagging rooms with WVDIs on the property website can better inform housing purchasers and renters' decision-making without entering every room in-person. For example, assuming similar housing prices, rooms on floors #2 may be first selected compared to ones on floors #3 due to high WVDIs. Rooms on floors #2 share similarly high WVDIs, and thus, other factors, e.g., indoor decorations, shall be emphasized.
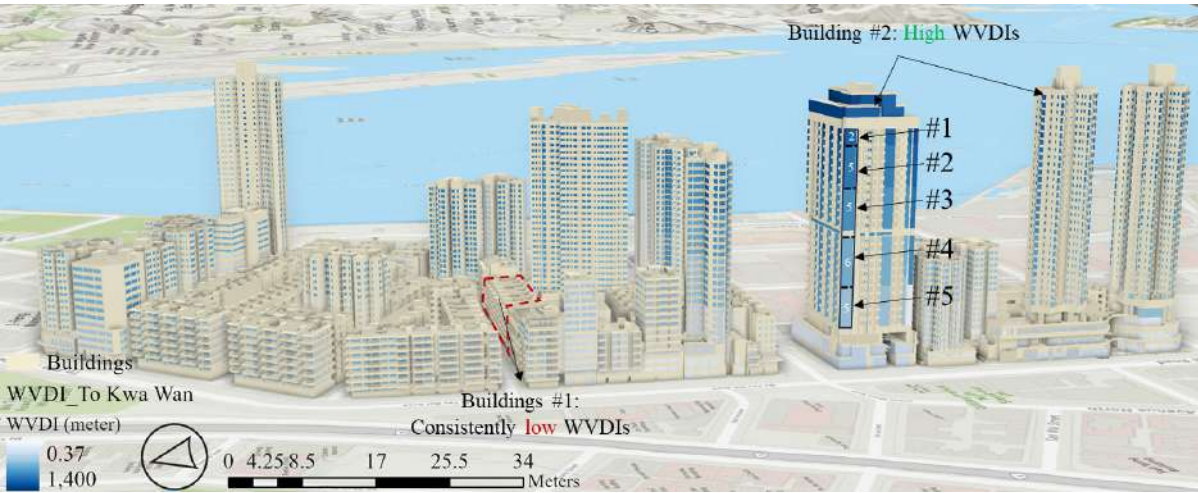


**Figure** 11. Visualized WVDIs of 207 example buildings in To Kwa Wan, Kowloon City District.

## 4.3 Sensitivity analysis

### 4.3.1 Performance of different 3D semantic segmentation methods

We examined five typical 3D semantic segmentation methods (see Table 2) with varied learning mechanisms for greenery detection. Overall, all five methods achieved satisfactory results, with Overall Accuracy (OA) above 97.55%, mean Accuracy (mAcc) above 96.08%, and mean Intersection over Union (mIoU) above 92.66%, respectively. StratifiedTransformer achieved the highest performance in distinguishing greenery and non-greenery, with Overall Accuracy (OA) at 98.38%, mean Accuracy (mAcc) at 97.26%, and mean Intersection over Union (mIoU) at 95.00%. Both greenery and non-greenery were classified with satisfactory per-class IoUs at 91.99% and 98.02%. The optimal performance benefits from the attention mechanism of the transformer and multi-scale receptive fields. Thus, the StratifiedTransformer was applied to estimate landscape types on CIMs in Sections 3.2.1 and experimental tests.

**Table** 2. Performances of five typical 3D semantic segmentation methods for greenery detection.

| Group | Deep learning method | Reference | Overall metric (%) | | | Per-class IoU (%) | |
|---|---|---|---|---|---|---|---|
| | | | OA | mAcc | mIoU | Greenery | Non-greenery |
| Voxel | SparseConvUnet | (Graham et al. 2018) | 97.55 | 96.62 | 92.66 | 88.31 | 97.00 |

| | | | | | | | | |
|---|---|---|---|---|---|---|---|---|
| 2D projection | BEV-Seg3D-Net | (Zou & Li 2021) | 97.64 | <u>96.08</u> | 92.82 | 88.52 | 97.12 |
| Kernel | KPConv | (Thomas et al. 2019) | 97.65 | 96.11 | 92.84 | 88.56 | 97.12 |
| Multilayer perceptron | RandLANet | (Hu et al. 2020) | 98.03 | 96.98 | 93.98 | 90.39 | 97.58 |
| Transformer | StratifiedTransformer | (Lai et al. 2022) | **98.38** | **97.26** | **95.00** | **91.99** | **98.02** |

Note: The highest and lowest values in each column are in bold and underlined, respectively.

410

### 4.3.2 Parameter setting of A-priori rules in estimating greenery subtypes

The thresholds $\beta$ and $\gamma$ were finetuned for the optimal performance of greenery subtype estimation. Referring to (HKEPD 2012), the height ranges of trees, shrubs, and grass are 2-15 m, less than 3-6 m, and 0.03-2 m, respectively. Thus, we set $\beta$ between 0.1 m and 1.9 m, and $\gamma$ between 2 m and 11 m to examine the detection performance. The evaluation metric is mIoU for detecting trees, shrubs, and grass on ten tiles of 250 m × 250 m annotated point clouds (see Figure 12b). Figure 12a shows the highest mIoU at 55.02% with $\beta = 0.9$ m and $\gamma = 4$ m. Tree was relatively well segmented, with IoU at 81.08%, whereas the detection of grass and shrub was poor, with IoUs at 53.49% and 30.49%, respectively. The primary reasons were the low-performance differentiation between the shrub and the

420 other two greenery subtypes, as well as minor mismatches in the input data caused by resolution variations, as illustrated in the rectangles in Figure 12b. Thus, we set $\beta = 0.9$ m and $\gamma = 4$ m in Section 4 to initially test the feasibility of our method.
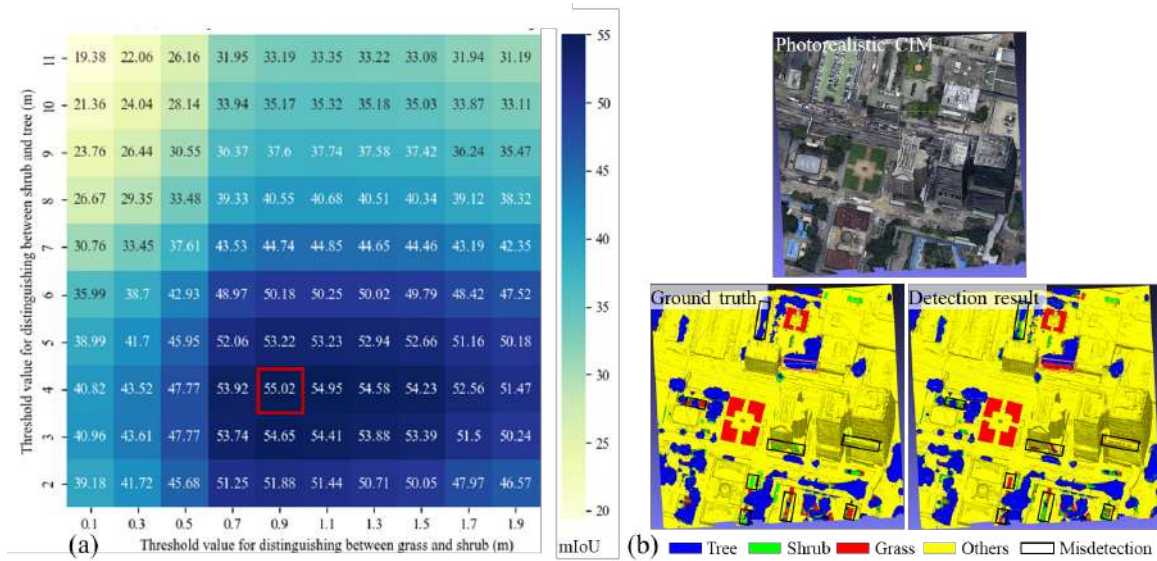


**Figure 12.** Finetuning height threshold values $\beta$ and $\gamma$. (a) Heatmap of mIoUs and (b) an example segmented CIM.

### 4.3.3 Parameter setting for visual permeability modeling of greenery

The WDVIs are adjustable to approach the ground truth of window view distances by controlling the greenery density $f$ in Eq. 3. In this study, we finetuned the greenery density parameters for trees, shrubs, and grass using two quality-varying CIMs reconstructed from varied proportions of the same

430     set of photogrammetric images (see Figure 13a). Compared to window view images generated from low-quality CIMs, the ones generated from high-quality CIMs offer a more accurate representation of window view distance. The reason is the detailed modeling of greenery and building envelopes. Thus, referring to WVDIs generated on high-quality CIMs as ground truth, we tested whether the finetuning of the greenery density parameter rendered the computed WVDIs on the low-quality CIMs more accurate. Specifically, we used the two CIMs to represent greenery while controlling other landscapes, e.g., buildings and roads, represented by the same high-quality CIM. By testing WVDIs on 20 window view images, Figure 13 shows the density parameters of trees, shrubs, and grass at 0.70, 0.80, and 0.90, respectively, achieving the most accurate WVDIs (RMSD = 0.17804). Compared to WVDIs computed on low-quality CIMs (RMSD = 1.86133), the finetuable greenery density

440     parameters increased the accuracy of the computed WVDIs by 90.43%. The result further confirmed that the proposed WVDIs and the automatic assessment method are accurate by precisely setting the greenery density parameters. Thus, we set the density parameters of trees, shrubs, and grass to 0.70, 0.80, and 0.90 for experimental tests in Section 4.
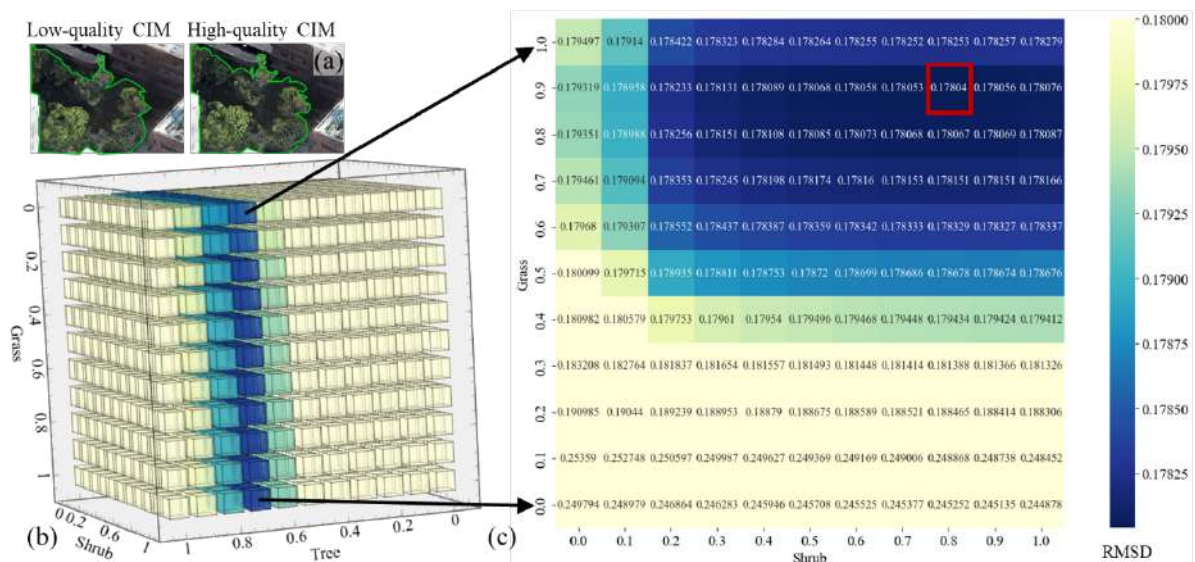


**Figure 13.** Finetuning parameters of greenery density. (a) Two CIMs of varying qualities, (b)-(c) 3D and 2D heatmaps of RMSDs.

## 5 Discussion

### 5.1 Significance and contribution

    Theoretically, the proposed study defines a novel WVDI on photorealistic CIMs regarding the visual

450     permeability of greenery. The WVDI, relating depth, landscape type, and greenery density, represents the average view distance between the window site and the visible landscape outside, addressing inaccuracy issues of traditional assessment via oversimplified solid surface modeling. Integrating Beer-Lambert's Attenuation Law (Swinehart 1962) in Physics, the presented WVDI extended the

modeling of visual permeability of greenery in GIS (Llobera 2007; Bartie et al. 2011) into window view assessment. The WVDI enables new solutions for multiple urban applications, e.g., precise housing valuation and transaction, prioritization of local urban density improvement, and optimization of window view openness for architectural and urban design.

Methodologically, the proposed study presents an accurate and efficient assessment method for window view distance using up-to-date photorealistic CIMs, 3D semantic segmentation, and OpenGL

460　rendering. By using type-depth window view nexus, the proposed method improves the efficiency of the traditional visibility analysis-based assessment method by 99.96%. For non-greenery window views, the computed WVDIs are close to the results of visibility analysis (RMSD ≤ 0.0002). For greenery window views, the WVDIs are more accurate (RMSD ≤ 0.1781), which effectively captures the potential view distance of greenery due to visual permeability. The high efficiency of the proposed method enables urban-scale quantification and updates of window view distances. The accurate assessment results support the decision-making of urban planners and designers in local urban density improvement, as well as developers, housing purchasers, and renters in real estate marketing.

## 5.2 Limitations and future work

The study has a few limitations. First, the accuracy of input parameters for estimating the view

470　distance of greenery requires improvement. There still exists room to improve the accuracy of 3D semantic segmentation for greenery subtypes, e.g., the tree, shrub, grass, and even more fine-grained species. Possible measurement errors exist in the view depth of the interior greenery due to photorealistic CIMs' continuous surface modeling. Future directions include the development of 3D CIM segmentation methods for accurately detecting greenery subtypes and the reconstruction of 3D volumetric and instantiated CIMs (Wu et al. 2024) for precise interior depth measurement. Second, the holistic semantic segmentation and rendering of CIMs can be costly for assessing window views at a small scale, e.g., for one building. Future directions include lightweight reconstruction of 3D CIMs for efficient 3D processing. Last, the presented WVDI is an objective metric without subjective calibration. Future directions include calibrating the WVDI via urban dwellers' perceptions and

480　landscape architects' knowledge to estimate window view quality and its human health and well-being benefits.

## 6 Conclusion

The scarcity of a distant view through the window leads to its amplified impacts on both urban health and real estate, especially in high-rise, high-density urban areas. Known benefits of distant window views from the literature include stress relief, living satisfaction, productivity improvement, and increased sense of privacy. As a big selling point, the distant window views of flats are also identified for profits in the real estate market. Thus, urban-scale assessment of window view distance is significant in examining the disparity of window view openness for prioritized built environment

improvement and precise housing valuation and transaction. Current studies are limited, inaccurate, and inefficient in assessing window view distance at the urban scale. To address the research gap, we present an automatic assessment of window view distance for high-rise, high-density urban areas using CIMs and 3D computer vision and graphics.

We first define a Window View Distance Index (WVDI) on a photorealistic CIM-generated window view image considering the visual permeability of greenery. Then, an automatic method was designed with three steps: i) landscape type estimation of photorealistic CIMs, ii) type-depth scene rendering, and iii) batch generation and quantification of window views for WVDIs. Last, we visualize the WVDIs on BIMs to support urban applications, e.g., local urban density improvement and informed housing valuation and transaction. Experimental results in Hong Kong Island and Kowloon Peninsula of Hong Kong showed that the method was automatic, efficient (2,753 times faster), and accurate (RMSD $\leq$ 0.1781) compared to the traditional visibility analysis-based method.

Our automatic assessment of window view distance enables new solutions for multiple applications and analytics in urban planning and design, real estate marketing, and urban health, thereby benefiting millions of urban dwellers. Examples include window view distance guided local urban density improvement via urban renewal, maximized achievement of window view distance for architectural and urban generative design, precise housing valuation and transaction, and a series of window view distance-based analytics for urban health and sustainability. Future work includes the development of 3D CIM segmentation methods for greenery subtype detection, reconstruction of 3D volumetric and instantiated CIMs for interior depth assessment, and lightweight reconstruction of 3D CIMs for efficient 3D semantic segmentation and rendering.

## Acknowledgement

## Authors' contribution roles

Maosu Li: Conceptualization, Data Collection and Processing, Methodology, Software, Validation, Charting, Writing – Original Draft Preparation, Funding Acquisition.

Fan Xue: Writing – Review and Editing, Funding Acquisition.

Anthony G. O. Yeh: Supervision, Writing – Review and Editing, Funding Acquisition.

# References

Bartie, P., Reitsma, F., Kingham, S. & Mills, S. (2011). Incorporating vegetation into visual exposure modelling in urban environments. *International Journal of Geographical Information Science, 25*(5), 851-868. doi:10.1080/13658816.2010.512273

CEN. (2018). *En 17037, Daylight in Buildings.* Brussels: Comité Européen de Normalisation (CEN).

Chung, W. K., Chau, C. K., Masullo, M. & Pascale, A. (2019). Modelling perceived oppressiveness and noise annoyance responses to window views of densely packed residential high-rise environments. *Building and Environment, 157*, 127-138. doi:10.1016/j.buildenv.2019.04.042

Fisher-Gewirtzman, D. (2018). Integrating 'weighted views' to quantitative 3D visibility analysis as a predictive tool for perception of space. *Environment and Planning B: Urban Analytics and City Science, 45*(2), 345-366. doi:10.1177/0265813516676486

Graham, B., Engelcke, M. & Van Der Maaten, L. (2018). 3d semantic segmentation with submanifold sparse convolutional networks. *Proceedings of the IEEE Conference on Computer Vision and Pattern Recognition* (pp. 9224-9232). New Jersey: IEEE. doi:10.1109/CVPR.2018.00961

HKEPD. (2012). *Tree Survey Data.* Hong Kong: Environmental Protection Department, Government of Hong Kong SAR. Retrieved from https://www.epd.gov.hk/eia/register/report/eiareport/eia_2032012/HTML/EIA%20Report/Annexes/Annex%20G_text.pdf

HKLandsD. (2020). *Hong Kong Digital Terrain Model from 2020 LiDAR Survey.* Hong Kong: Lands Department, Government of Hong Kong SAR.

HKLandsD. (2023). *iB1000 Digital Topographic Map.* Hong Kong: Lands Department, Government of Hong Kong SAR.

HKPlanD. (2018). *Hong Kong Planning Standards and Guidelines.* Hong Kong: Planning department, Hong Kong SAR. doi:https://www.pland.gov.hk/pland_en/tech_doc/hkpsg/full/pdf/ch2.pdf

HKPlanD. (2019). *3D Photo-realistic Model.* Hong Kong: Planning Department, Government of Hong Kong SAR. Retrieved from https://www.pland.gov.hk/pland_en/info_serv/3D_models/download.htm

HKURA. (2022). *3D Intelligent Map of An Area in To Kwa Wan.* Hong Kong: Hong Kong Urban Renewal Authority.

Hu, Q., Yang, B., Xie, L., Rosa, S., Guo, Y., Wang, Z., Trigoni, N. & Markham, A. (2020). RandLA-Net: Efficient semantic segmentation of large-scale point clouds. *Proceedings of the*

530

540

550

*IEEE/CVF Conference on Computer Vision and Pattern Recognition* (pp. 11108-11117). New Jersey: IEEE. doi:10.1109/CVPR42600.2020.01112

Huang, J. (2019). *A 3D GIS-based Valuation System for Assessing the Scenic View in Residential Property Valuations [PhD thesis].* Hong Kong: The Hong Kong Polytechnic University. Retrieved from https://theses.lib.polyu.edu.hk/handle/200/9974

Inglis, N. C., Vukomanovic, J., Costanza, J. & Singh, K. K. (2022). From viewsheds to viewscapes: Trends in landscape visibility and visual quality research. *Landscape and Urban Planning, 224*, 104424. doi:10.1016/j.landurbplan.2022.104424

IWBI. (2020). *Well V2 - the Next Version of the Well Building Standard.* New York: International Well Building Institute. Retrieved from https://v2.wellcertified.com/en/wellv2/overview

Kent, M. & Schiavon, S. (2020). Evaluation of the effect of landscape distance seen in window views on visual satisfaction. *Building and Environment, 183*, 107160. doi:10.1016/j.buildenv.2020.107160

Kim, J., Kent, M., Kral, K. & Dogan, T. (2022). Seemo: A new tool for early design window view satisfaction evaluation in residential buildings. *Building and Environment, 214*, 108909. doi:10.1016/j.buildenv.2022.108909

Ko, W. H., Kent, M. G., Schiavon, S., Levitt, B. & Betti, G. (2022). A window view quality assessment framework. *Leukos, 18*(3), 268-293. doi:10.1080/15502724.2021.1965889

Lai, X., Liu, J., Jiang, L., Wang, L., Zhao, H., Liu, S., Qi, X. & Jia, J. (2022). Stratified transformer for 3d point cloud segmentation. *Proceedings of the IEEE/CVF Conference on Computer Vision and Pattern Recognition* (pp. 8500-8509). New Jersey: IEEE. doi:10.1109/CVPR52688.2022.00831

Laovisutthichai, V., Li, M., Xue, F., Lu, W., Tam, K. & Yeh, A. G. (2021). CIM-enabled quantitative view assessment in architectural design and space planning. *38th International Symposium on Automation and Robotics in Construction (ISARC 2021)* (pp. 65-72). Oulu: IAARC.

Li, M., Wu, Y., Yeh, A. G. & Xue, F. (2023a). HRHD-HK: A benchmark dataset of high-rise and high-density urban scenes for 3D semantic segmentation of photogrammetric point clouds. *2023 IEEE International Conference on Image Processing Challenges and Workshops (ICIPCW)* (pp. 3714-3718). New Jersey: IEEE. doi:10.1109/ICIPC59416.2023.10328383

Li, M., Xue, F. & Yeh, A. G. (2023b). Efficient assessment of window views in high-rise, high-density urban areas using 3D color city information models. *Proceedings of the 18th*

*International Conference on Computational Urban Planning and Urban Management* (pp. 1-11). Charlottesville: OSF. doi:10.17605/OSF.IO/6YR5V

Li, M., Xue, F., Wu, Y. & Yeh, A. G. (2022). A room with a view: Automated assessment of window views for high-rise high-density areas using City Information Models and transfer deep learning. *Landscape and Urban Planning, 226*, 104505. doi:10.1016/j.landurbplan.2022.104505

Li, M., Xue, F., Yeh, A. G. & Lu, W. (2021). Classification of photo-realistic 3D window views in a high-density city: The case of Hong Kong. In X. Lu, Z. Zhang, W. Lu & Y. Peng, *Proceedings of the 25th International Symposium on Advancement of Construction Management and Real Estate* (pp. 1339-1350). Singapore: Springer.

Li, M., Yeh, A. G. & Xue, F. (2024). CIM-WV: A 2D semantic segmentation dataset of rich window view contents in high-rise, high-density areas based on photorealistic City Information Models. *Urban Informatics, 3*, 1-24.

Liang, D., Chen, S. H., Chen, Z., Wu, Y., Chu, L. Y. & Xue, F. (2024). 4D point cloud-based spatial-temporal semantic registration for monitoring mobile crane construction activities. *Automation in Construction, 165*, 105576. doi:10.1016/j.autcon.2024.105576

Lin, T.-Y., Le, A.-V. & Chan, Y.-C. (2022). Evaluation of window view preference using quantitative and qualitative factors of window view content. *Building and Environment, 213*, 108886. doi:10.1016/j.buildenv.2022.108886

Ling, Y. (2022). Estimating coastal premiums for apartment prices: Towards a new multilevel modelling approach. *Environment and Planning B: Urban Analytics and City Science, 49*(1), 188-205. doi:10.1177/23998083211000343

Llobera, M. (2007). Modeling visibility through vegetation. *International Journal of Geographical Information Science, 21*(7), 799-810. doi:10.1080/13658810601169865

Luo, L. & Jiang, B. (2022). From oppressiveness to stress: A development of Stress Reduction Theory in the context of contemporary high-density city. *Journal of Environmental Psychology, 84*, 101883. doi:10.1016/j.jenvp.2022.101883

Masoudinejad, S. & Hartig, T. (2020). Window view to the sky as a restorative resource for residents in densely populated cities. *Environment and Behavior, 52*(4), 401-436. doi:10.1177/0013916518807274

McPhail, R., Chan, X. W., May, R. & Wilkinson, A. (2024). Post-COVID remote working and its impact on people, productivity, and the planet: an exploratory scoping review. *The*

*International Journal of Human Resource Management, 35*(1), 154-182.
doi:10.1080/09585192.2023.2221385

Meng, S., Su, X., Sun, G., Li, M. & Xue, F. (2025). From 3D pedestrian networks to wheelable networks: An automatic wheelability assessment method for high-density urban areas using contrastive deep learning of smartphone point clouds. *Computers, Environment and Urban Systems, 117*, 102255. doi:10.1016/j.compenvurbsys.2025.102255

Mistick, K. A., Campbell, M. J., Thompson, M. P. & Dennison, P. E. (2023). Using airborne lidar and machine learning to predict visibility across diverse vegetation and terrain conditions. *International Journal of Geographical Information Science, 37*(8), 1728-1764. doi:10.1080/13658816.2023.2224421

Murgoitio, J. J., Shrestha, R., Glenn, N. F. & Spaete, L. P. (2013). Improved visibility calculations with tree trunk obstruction modeling from aerial LiDAR. *International Journal of Geographical Information Science, 27*(10), 1865-1883. doi:10.1080/13658816.2013.767460

Qi, J., Lin, E. S., Tan, P. Y., Ho, R. C., Sia, A., Olszewska-Guizzo, A., Zhang, X. & Waykool, R. (2022). Development and application of 3D spatial metrics using point clouds for landscape visual quality assessment. *Landscape and Urban Planning, 228*, 104585. doi:10.1016/j.landurbplan.2022.104585

Ruzickova, K., Ruzicka, J. & Bitta, J. (2021). A new GIS-compatible methodology for visibility analysis in digital surface models of earth sites. *Geoscience Frontiers, 12*(4), 101109. doi:10.1016/j.gsf.2020.11.006

Stamps III, A. E. (2011). Effects of area, height, elongation, and color on perceived spaciousness. *Environment and Behavior, 43*(2), 252-273. doi:10.1177/0013916509354696

Swinehart, D. F. (1962). The beer-lambert law. *Journal of Chemical Education, 39*(7), 333-335.

Thomas, H., R. Qi, C., Deschaud, J.-E., Marcotegui, B., Goulette, F. & Guibas, L. J. (2019). Kpconv: Flexible and deformable convolution for point clouds. *Proceedings of the IEEE/CVF International Conference on Computer Vision* (pp. 6411-6420). New Jersey: IEEE. doi:10.1109/ICCV.2019.00651

Tong, Z., Yang, H., Liu, C., Xu, T. & Xu, S. (2020). Quantification of the openness of urban external space through urban section. *Geo-spatial Information Science, 23*(4), 316-326. doi:10.1080/10095020.2020.1846464

Ulrich, R. S. (1984). View through a window may influence recovery from surgery. *Science, 224*(4647), 420-421. doi:10.1126/science.6143402

van Esch, E., Minjock, R., Colarelli, S. M. & Hirsch, S. (2019). Office window views: View features trump nature in predicting employee well-being. *Journal of Environmental Psychology, 64*, 56-64. doi:10.1016/j.jenvp.2019.05.006

Wang, B., Li, M., Peng, Z. & Lu, W. (2024). Hierarchical attributed graph-based generative façade parsing for high-rise residential buildings. *Automation in Construction, 164*, 105471. doi:10.1016/j.autcon.2024.105471

Wang, B., Lu, W. & Zhang, Y. (2025). A graph-enabled parametric modeling approach for façade layout generative design. *Journal of Building Engineering, 105*, 112481. doi:10.1016/j.jobe.2025.112481

Wang, F. & Munakata, J. (2024). Assessing the impact of facade characteristics and visual elements on perceived oppressiveness in high-rise window views through virtual reality. *Building and Environment, 266*, 112043. doi:10.1016/j.buildenv.2024.112043

Wu, Y., Xue, F., Li, M. & Chen, S. H. (2024). A novel Building Section Skeleton for compact 3D reconstruction from point clouds: A study of high-density urban scenes. *ISPRS Journal of Photogrammetry and Remote Sensing, 209*, 85-100. doi:10.1016/j.isprsjprs.2024.01.020

Yamagata, Y., Murakami, D., Yoshida, T., Seya, H. & Kuroda, S. (2016). Value of urban views in a bay city: Hedonic analysis with the spatial multilevel additive regression (SMAR) model. *Landscape and Urban Planning, 151*, 89-102. doi:10.1016/j.landurbplan.2016.02.008

Yao, T., Lin, W., Bao, Z. & Zeng, C. (2024). Natural or balanced? The physiological and psychological benefits of window views with different proportions of sky, green space, and buildings. *Sustainable Cities and Society, 104*, 105293. doi:10.1016/j.scs.2024.105293

Zhang, F., Salazar-Miranda, A., Duarte, F., Vale, L., Hack, G., Chen, M., Liu, Y., Batty, M. & Ratti, C. (2024). Urban Visual Intelligence: Studying Cities with Artificial Intelligence and Street-Level Imagery. *Annals of the American Association of Geographers , 114*(5), 876-897. doi:10.1080/24694452.2024.2313515

Zhu, H., Yang, X., Zhou, X., Zhang, H., Yang, L. & Tang, G. (2024). A 3D visible space index for evaluating urban openness based on the digital urban model. *International Journal of Geographical Information Science*, 1-26. doi:10.1080/13658816.2024.2397434

Zong, X., Wang, T., Skidmore, A. K. & Heurich, M. (2021). The impact of voxel size, forest type, and understory cover on visibility estimation in forests using terrestrial laser scanning. *GIScience & Remote Sensing, 58*(3), 323-339. doi:10.1080/15481603.2021.1873588

Zou, Z. & Li, Y. (2021). Efficient urban-scale point clouds segmentation with bev projection. (pp. 1-6). arXiv preprint. doi:arXiv:2109.09074

680